

Surge Instability on a Cavitating Propeller

By M. E. DUTTWEILER[†] AND C. E. BRENNEN

Division of Engineering and Applied Science,
California Institute of Technology, Pasadena, California

(Received October 2000)

This study details experiments investigating a previously unrecognized surge instability on a cavitating propeller in a water tunnel. The surge instability is explored through visual observation of the cavitation on the propeller blades and in the tip vortices. Similarities between the instability and previously documented cavitation phenomena are noted. Measurements of the radiated pressure are obtained, and the acoustic signature of the instability is identified. The magnitudes of the fluctuating pressures are very large, presumably capable of producing severe hull vibration on a ship.

The origins of this instability are explored through separate investigation of the cavitation dynamics and the response of the water tunnel to volumetric displacement in the working section. Experiments are conducted to quantify the dynamics of the propeller cavitation. Finally, a model is developed for the complete system, incorporating both the cavitation and facility dynamics. The model predicts active system dynamics (linked to the mass flow gain factor familiar in the context of pump dynamics) and therefore potentially unstable behavior for two distinct frequency ranges, one of which appears to be responsible for the instability.

1. Introduction

Experimental experience and theoretical analyses have revealed that the adverse effects of cavitation are often augmented under unsteady flow conditions. The fluctuations of the cavitation volume on a ship's propeller, for example, can cause severe and often structurally damaging vibrations to the hull at the aft end of the ship. Because of this and related problems in pumps, turbines, and other potentially cavitating devices, there is a clear need to understand unsteady phenomena and instabilities connected to cavitating flows.

One such phenomenon is the partial cavity instability on a single hydrofoil or cascade of hydrofoils (Wade and Acosta 1966, Franc and Michel 1988, Le, Franc and Michel 1993, de Lange, de Bruin & van Wijngaarden 1994). The behavior of hydrofoils subject to forced oscillation in pitch about a spanwise axis has also been the subject of much research. Many investigators (Shen and Peterson 1978, Franc and Michel 1988, Hart *et al.* 1990, Soyama *et al.* 1992, McKenney and Brennen 1994, Reisman *et al.* 1998) have examined the periodic formation and collapse of clouds of cavitation bubbles on the suction surface of hydrofoils or pump blades and the very large transient pressure pulses and severe structural damage that can result.

Until very recently, the great majority of this work focused on the behavior of two-dimensional, unswept hydrofoils. However, the recent observations of attached cavities on hydrofoils with sweep by Jessup (1997) and Laberteaux and Ceccio (1998) have identified

[†] Present address: Applied Minds Inc., 655 N. Central Avenue, Glendale, California

some notable differences between the cavitation on swept and unswept hydrofoils and these will be referred to below.

Implicitly assumed in many of these investigations is that the phenomena observed within the laboratory facilities accurately reflect the cavitation behavior of devices operating in more open conditions. Only a few studies (Shen and Peterson 1978, Kjeldsen *et al.* 1999) have considered the interactions between the dynamics of the unsteady cavitation and the dynamics of the surrounding experimental facility.

This is not the case for cavitating pumps, where for some time the dynamics of the pump cavitation and the response of the surrounding facility have been known to interact with very dramatic consequences, including the catastrophic POGO instability observed in liquid-propelled rockets. A great deal of research has therefore been focused on quantifying the cavitation dynamics involved in oscillations of this nature. A relatively consistent approach has been adopted, with efforts aimed at developing a transfer matrix characterizing the relationship between the fluctuating pressure and mass flow rate at the pump inlet and the same quantities at discharge. This transfer matrix summarizes the dynamic behavior of the pump, including the cavitation. In determining the elements of this transfer matrix, two important parameters were identified. The cavitation compliance models the effective compressibility of the cavitating flow between the inlet and outlet (Brennen and Acosta 1973) and was shown to play an important role in several observed hydraulic system instabilities. A second factor, the mass flow gain factor, represents the response of the cavitation to variations in the inlet mass flow rate (Brennen and Acosta 1976). It was later demonstrated (Brennen 1978, Tsujimoto *et al.* 1993) that this parameter, for which a typically positive value implies an increase in cavitation volume with decreasing inlet mass flow rate, is a key factor in sustaining instabilities in cavitating pumps. One such instability is the “auto-oscillation” of cavitating inducers, in recent years renamed cavitation surge (Braisted & Brennen 1978, 1980). The first attempts to experimentally measure the mass flow gain factor as well as the cavitation compliance and the other components of the transfer matrix were performed by Ng and Brennen (1978), with more precise measurements later obtained by Brennen *et al.* (1982). More recently, the frequency dependence of the mass flow gain factor has been explored theoretically by Otsuka *et al.* (1996).

The majority of investigations exploring the unsteady cavitating behavior of propellers as opposed to pumps has focused on the consequences of the varying inflow encountered by a propeller blade as it rotates through the irregular wake behind a ship hull. Huse (1972) was the first to explore the resulting variations in cavity volume and their effect on the pressures radiated by the cavitation. The amplitude of the pressure fluctuations and the induced vibrations of the ship hull were found to be orders of magnitude greater than for the case of steady cavitating flow. An excellent summary of the large body of work focused on the propeller-hull vibration problem is offered in Weitendorf (1989). A discussion of the various unsteady cavitation structures that can result from the irregular wake is presented by Bark (1986). McKenney (1995) explored the unsteady flow field encountered by a yawed propeller and its effect on tip vortex cavitation.

Few if any cavitating propeller investigations have adopted an approach similar to the cavitating pump analyses and explored the possible interaction between unsteady propeller cavitation and the dynamics of the surrounding environment. The goal of this work is to utilize concepts garnered from general unsteady cavitation research and extend several more specific concepts from investigations of cavitating pump instabilities to describe and explain a previously unobserved cavitation surge instability on a propeller.

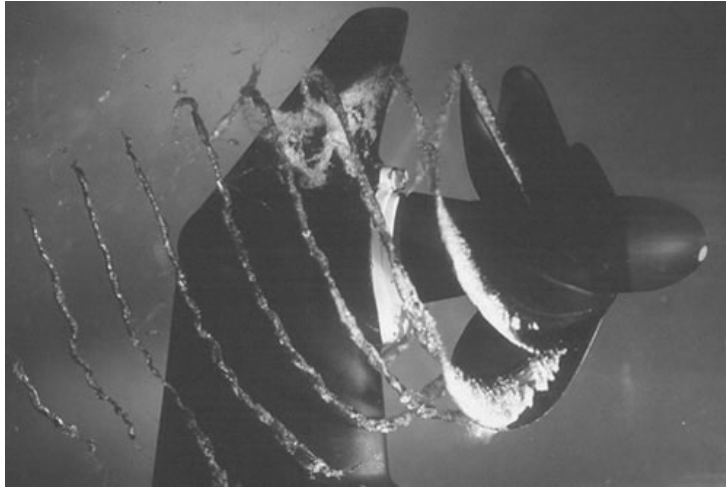


FIGURE 1. Photograph of stable cavitation with the propeller operating upstream of the gear case at $\beta = 0^\circ$, $n = 28.3 \text{ Hz}$, $J = 0.68$, and $\sigma = 0.19$.

2. Propeller Cavitation Surge Observations

A 190.5 mm diameter model propeller typical of the modern designs used by the U.S. Navy was installed in the Low Turbulence Water Tunnel (LTWT) at Caltech (Gates 1977) using a transverse shaft and gear box taken from an outboard motor (see figure 1 and McKenney 1995). The fairing around the shaft and gearbox was quite streamlined. The entire assembly could be rotated about its base so as to operate the propeller either upstream of downstream of the fairing.

Experiments began with the propeller mounted upstream of the fairing, as shown in the photograph of figure 1. Later, when the propeller was operated downstream of the fairing, a violent surge instability was observed to occur in certain regimes of operation. The instability was characterized by a periodic increase and decrease in the extent of cavitation both on the propeller blades and in the tip vortices shed downstream. This fluctuation in cavitation extent was readily apparent to the naked eye, and occurred evenly and synchronously on all blades and at all angular locations. The resulting pressure fluctuations were dramatic, easily audible to the unaided ear, and propagated throughout the surrounding experimental facility. The instability was observed across the range of propeller rotation speeds at which the cavitating conditions could be achieved, $n = 28.3 - 31.7 \text{ Hz}$. The frequency of the fluctuation was repeatable and in the range $f = 9 - 11 \text{ Hz}$. The variation of the fluctuation frequency with the basic flow parameters is discussed in greater detail in Duttweiler (2001).

2.1. Visual Observations

Figure 2 presents selected frames from high speed video footage of the instability on the cavitating propeller. The number indicated in each frame corresponds to the fraction, τ , of the instability cycle elapsed. The beginning of the instability cycle is chosen arbitrarily to coincide with the minimum cavitation extent. This condition, as seen in the first frame of figure 2, is characterized by a relatively small region of bubbly cavitation along the leading edge of the propeller blade.

Further into the instability cycle, at $\tau = 0.25$, the cavity has grown substantially towards the trailing edge of the propeller blade. A re-entrant jet becomes distinguishable as it is swept back from the leading edge, its forward front indicated by the white arrow.

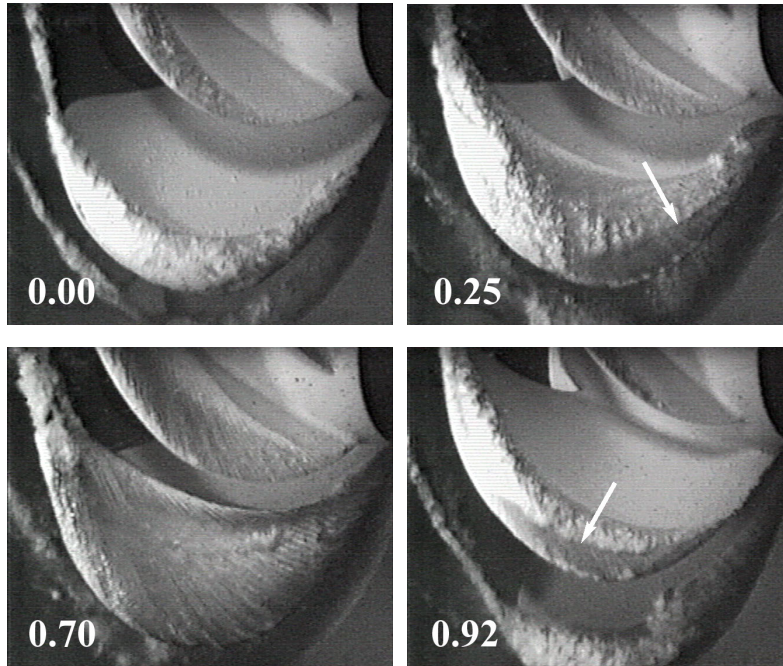


FIGURE 2. Four frames taken from a high speed video, showing the variation in cavitation on an individual propeller blade during the instability cycle. The number in the lower left corner of each frame, τ , indicates the fraction of the instability cycle elapsed. The white arrow indicates the front of the re-entrant jet.

The cavity reaches its maximum extent at approximately $\tau = 0.70$. At this stage of the instability cycle, a supercavitating condition occurs when the cavity near the tip of the propeller blade extends downstream of the trailing edge of the blade. As this cavitation is entrained into the tip vortices it leads to a readily observed increase in the diameter of the vortices shed downstream of the propeller. No re-entrant jet is visible at this point in the cycle, presumably because the jet fluid has been swept past the cavity closure region.

By $\tau = 0.92$ the cavitation has begun to decrease in extent, receding towards the leading edge of the propeller blades. The re-entrant jet can again be observed, indicated by the white arrow, as it begins its rush forward within the cavity towards the leading edge of the propeller. When the re-entrant jet reaches the leading edge at nearly all spanwise locations, the cavitation returns to the minimal configuration shown at $\tau = 0.00$.

While no record of an instability of this nature could be found in the literature, the nature of the cavitation in figure 2 exhibits some similarities to observations made by previous investigators characterizing the cavitation on three-dimensional, swept hydrofoils. In particular, Jessup (1997) and Laberteaux and Ceccio (1998) noted that the re-entrant flow on swept hydrofoils was not directed upstream as in the case of a similar unswept hydrofoil, but was instead obliquely inclined to the line of cavity closure. Furthermore, they observed that the cavity closure downstream and outboard of the location where the re-entrant flow impinged upon the leading edge of the hydrofoil was rough and unsteady. A similar effect can be seen in the third image of figure 2, where the cavitation is particularly frothy downstream and outboard (above and to the left) of the point at which the re-entrant jet reaches the leading edge.

Also evident from figure 2 are similarities between the instability cycle and the well documented partial cavity instability observed on two-dimensional hydrofoils (Wade and

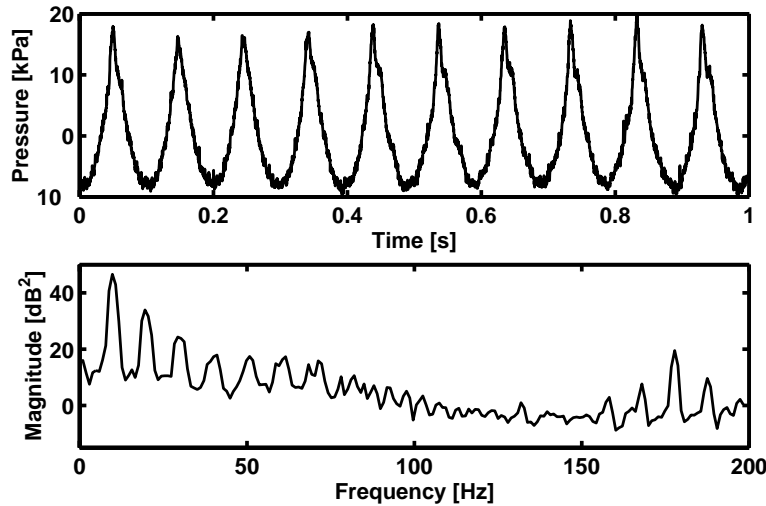


FIGURE 3. Typical pressure measurements obtained from the floor-mounted pressure transducer during the instability. The signal was low-pass filtered at 2 kHz . Also shown is an average power spectral density obtained from several such signals.

Acosta 1966, Franc and Michel 1988, Le, Franc and Michel 1993, deLange *et al.* 1994). First, the cavity length on the propeller blade is fluctuating between two very different but consistent values. Furthermore, the cavity lengths about which the fluctuation occurs are comparable to the chord length, c , of the propeller blade. Finally, the frequency, f , of the fluctuation is quite low. Wade and Acosta (1966) reported reduced frequencies, $k = fc/U$, based on chord length and incoming flow velocity, U , in the range $k = 0.07 - 0.14$. Le, Franc and Michel (1993) and de Lange *et al.* (1994) encountered somewhat higher values of approximately $k = 0.34$. If reduced frequencies for the propeller based on chord length and incident velocity are computed at various radii, values of the order of $k = 0.07$ are obtained. These are consistent with the range reported by Wade and Acosta (1966), but somewhat lower than the value reported by the other investigators.

2.2. Pressure Measurements

To further quantify the instability, pressure measurements were taken using a pressure transducer flush-mounted in the floor of the water tunnel test section, approximately even with the propeller in a streamwise direction and 15 cm below the axis of propeller rotation. A typical signal obtained from the floor-mounted transducer is shown in figure 3. The signal is clearly periodic, with a frequency corresponding to the frequency of cavitation variation observed visually. The magnitude of the pressure oscillations produced by the instability was as high as $15 - 20\text{ kPa}$, at least one order of magnitude higher than the cavitation noise radiated under stable conditions. These pressure oscillations were strong enough to be readily heard in the laboratory and to shake the test section violently.

Also shown in figure 3 is an average of several power spectral densities of the pressures generated by the instability. Clearly visible at approximately 10 Hz is the fundamental frequency of the instability, dominating the instability noise by a margin of approximately 15 dB . Many harmonics can also be seen. The blade passage frequency for the six bladed propeller rotating at $n = 30.0\text{ Hz}$ is also clear as are two beat frequencies at 170 Hz and 190 Hz .

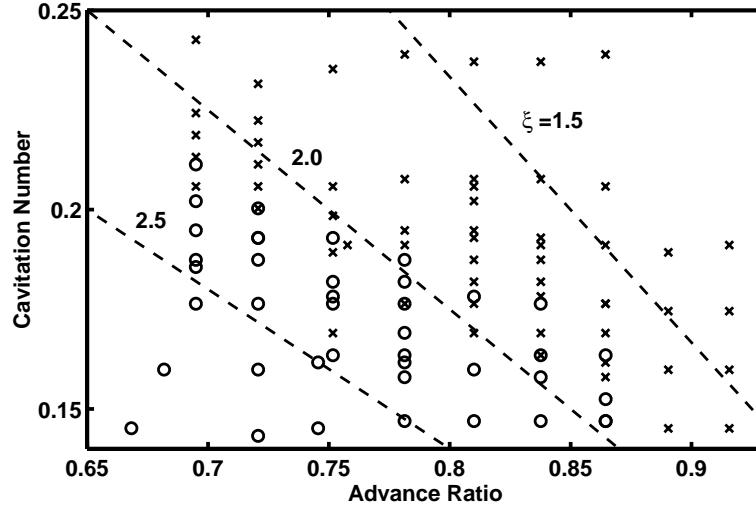


FIGURE 4. Occurrence of the instability in a cavitation number and advance ratio map. Each operating point is classified as stable (\times), unstable (\circ), or marginally stable (\otimes). The propeller rotation speed in this case was $n = 30.8 \text{ Hz}$. The dashed lines ($--$) are for different values of the parameter ξ , and correspond to the stability criterion discussed in the text.

2.3. Onset of Instability

The onset of the instability was difficult to define precisely. However, if spectra were obtained at decreasing cavitation numbers, a transition in the spectra was observed between a dominant peak near $f = 14 \text{ Hz}$ to a value near $f = 9 \text{ Hz}$. This growth of the lower frequency peak was utilized in defining the onset of instability. Following this onset, the frequency of the dominant peak remained constant with increasing intensity of the instability.

Figure 4 summarizes the onset of the instability in an advance ratio and cavitation number map. The unstable operating conditions are concentrated at advance ratios, J , below the design advance ratio of $J_o = 1.15$, and at lower cavitation numbers. Some insight regarding the onset of the instability can be gained by considering following argument. Studies of two-dimensional foils, for example by Tulin (1953) (see also Brennen 1995), have shown that the non-dimensional cavity length, l/c , is essentially a function of the ratio, α/σ , of the angle of attack of the hydrofoil, α , to the cavitation number, σ . Based on purely geometric arguments, the angle of attack in the vicinity of a propeller blade tip is approximately proportional to the difference, $J_o - J$, between the design advance ratio, J_o (1.15 in the present case), and the operating advance ratio, J . Thus a particular configuration of cavity lengths on the propeller should correspond to a particular value of the parameter $\xi = (J_o - J)/\sigma$.

Several lines of constant ξ are plotted in figure 4 where it is clear that the transition between stable and unstable behavior corresponds quite closely to the particular value of $\xi = 2.0$. Thus the instability boundary corresponds to a particular configuration of cavity lengths on the propeller blade. This confirms the connection with the partial cavity instability observed on two-dimensional foils, where stability was also related to the ratio of cavity length to chord.

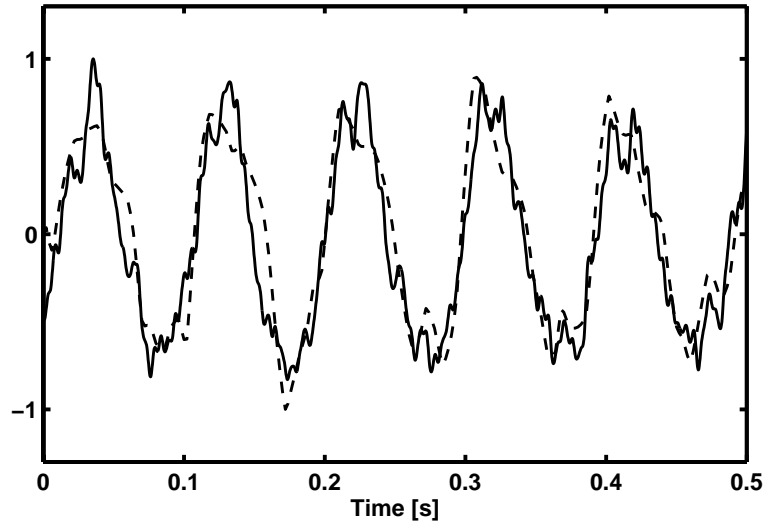


FIGURE 5. A comparison between the signal from the floor-mounted pressure transducer low-pass filtered at 200 Hz (—) and the second time derivative of the measured cavity volume (---). The vertical scales are arbitrary.

2.4. Modeling the Instability Pressures

As suggested by Huse (1972), the far field pressure from a fluctuating cavity volume will be dominated by the volumetric acceleration imposed upon the flow. Specifically,

$$\tilde{p} \sim \frac{d^2 \tilde{V}_{cav}}{dt^2} \quad (2.1)$$

where \tilde{p} is the fluctuating far field pressure and \tilde{V}_{cav} is the fluctuating cavity volume. This volumetric acceleration was determined from direct measurements of the cavity volume throughout the instability cycle in the following way. High speed video footage similar to that shown in figure 2 was obtained, and synchronized by a timing pulse with measurements from the floor-mounted pressure transducer. Frames of the video footage were then digitally captured and analyzed. In each frame, the cavitation extent varied substantially with radial location, but was most easily characterized by the maximum value of a cavity length, l , measured normal to the leading edge. From this cavity length measurement, an estimate of the cavity volume was obtained by following the suggestion of Blake (1986) that $V_{cav} \sim Rl^2$, where R is the propeller radius.

A finite difference method was then applied to the cavity volume estimates to determine the second time derivative of cavity volume and therefore the volumetric acceleration imposed upon the flow. Figure 5 shows the results of this calculation and the comparison with the pressure measurements obtained from the floor-mounted transducer. Note that the qualitative agreement between the two is very good even in some of the higher frequency details. However, we also note that the vertical scales in figure 5 have been arbitrarily chosen to facilitate the comparison. As will be seen, quantitative comparison requires detailed knowledge of the response of the facility.

3. Facility Dynamics

To estimate the amplitude of the pressures generated by the instability, a model is needed to describe the response of the system to the fluctuating flow rates and pressures

produced by the cavitating propeller. One very simple approach would be to model the propeller cavitation as a monopole source from which the generated pressures decay as r^{-2} , where r is the distance from the cavity. This proved wholly inadequate in predicting the amplitudes of the pressures observed at the floor-mounted transducer. To fully understand the pressures generated by the instability, a model is needed that will incorporate the effect on the pressure of the dynamic response of the experimental facility.

3.1. Lumped Parameter System Impedance

In developing the model, it is assumed that the facility responds linearly to the perturbations in the flow conditions; non-linear considerations are currently beyond our capability. Accordingly, the quantities of interest are expressed as a linear combination of a mean component and a fluctuating component of frequency ω . The mass flow rate and the resulting total pressure are therefore denoted by

$$m = \bar{m} + \text{Re}[\tilde{m}e^{j\omega t}] \quad ; \quad p^T = \bar{p}^T + \text{Re}[\tilde{p}^T e^{j\omega t}] \quad (3.1)$$

where \bar{m} and \bar{p}^T are the time-averaged mass flow rate and total pressure. The fluctuating components \tilde{m} and \tilde{p}^T are complex, in order to incorporate both the amplitude and phase of the fluctuations.

The dynamics of the facility can be characterized by considering the response of the facility to a fluctuating mass flow rate, \tilde{m}_e , injected at some specific location e in the system (figure 6). We define a system impedance,

$$Z = \frac{\tilde{p}_e^T}{\tilde{m}_e} \quad (3.2)$$

where, in general, Z is complex, and its value depends on the location of the excitation point, e .

To develop a specific expression for the system impedance, Z , we employ a lumped parameter approach, dividing the experimental facility into smaller components exhibiting resistive, inertive, and compliant behavior. The details of this analysis are given in Duttweiler (2001). The facility dynamics are characterized by (1) the compliance, C_{ot} , of the overflow tank that allows control of the pressure within the facility and therefore has the only deliberate free surface, (2) the resistance, R_c , and inertance, L_c , of the pipe leading from the tunnel to this overflow tank, (3) the compliance, C_t , associated with the expansion and contraction of the walls of the tunnel, and (4) the resistances, R_{tu} and R_{td} , and inertances, L_{tu} and L_{td} , associated with the typical flow paths leading from the point of excitation to the location of the expanding and contracting walls. The resulting model is shown in figure 6. It is necessarily a crude approximation to what is a much more complex dynamic system but appears to contain all the elements required for present purposes.

Several of these lumped parameters can be evaluated directly from measurements of the experimental facility. The overflow tank compliance is composed of contributions from the motion of the free surface and the compression of the sealed volume of air above the free surface, so that

$$C_{ot}^{-1} = \left\{ \frac{\bar{A}_{ot}}{g} \right\}^{-1} + \left\{ \frac{\rho \bar{V}_{ot}}{\bar{p}_{ot} k} \right\}^{-1} = C_{fs}^{-1} + C_{sv}^{-1} \quad (3.3)$$

where \bar{A}_{ot} is the area of the free surface of the overflow tank, g is the acceleration due to gravity, and \bar{V}_{ot} , \bar{p}_{ot} , and k are the unperturbed volume, pressure, and polytropic constant of the air volume above the overflow tank free surface. The connecting pipe inertance, L_c , can be evaluated directly from the connecting pipe length and area. Similarly, the

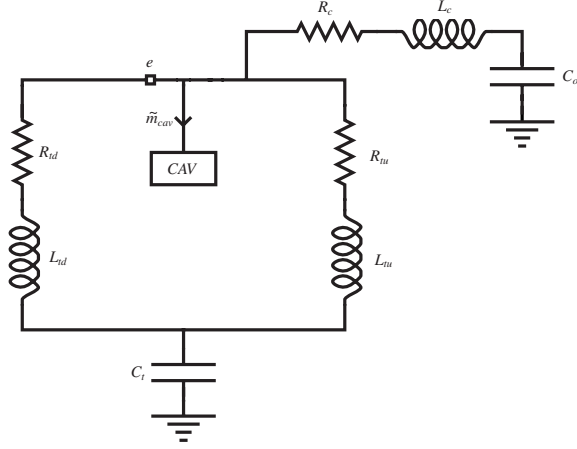


FIGURE 6. Schematic of facility and cavitation dynamics.

tunnel inertances, L_{tu} and L_{td} , can be estimated by considering the length and varying cross-sectional area of the typical flow paths between the excitation point and the tunnel compliance.

The remaining parameter, the tunnel compliance associated with the expansion and contraction of the tunnel walls, is difficult to evaluate directly, but can be estimated by measuring the quasistatic response of the tunnel walls to changes in internal pressure. Figure 7 shows the results from such an experiment. Clearly the deflection varies greatly with location. It is probable that other locations around the tunnel exterior, where material, and size, shape, and extent of reinforcement vary widely, would also show similar variation. Nonetheless, it is possible to estimate from figure 7 a range of values for the tunnel compliance. Considering the definition of the compliance,

$$C_t \doteq \rho \frac{dV_t}{dp_t} = \rho \frac{dV_t}{ds} \frac{ds}{dp_t} \quad (3.4)$$

where ds/dp_t is the slope of figure 7, and dV_t/ds is simply the surface area of the tunnel. Estimating the latter to be 75 m^2 , we judge that

$$7.5 \times 10^{-5} \text{ ms}^2 \leq C_t \leq 1.5 \times 10^{-3} \text{ ms}^2 \quad (3.5)$$

3.2. Natural Frequency Experiments

Neglecting the resistive components in the system, the impedance at the point e of figure 6 just downstream of the cavitating propeller is given by

$$Z = \frac{j(L_c C_{ot} w^2 - 1)(L_t C_t w^2 - 1)}{w[(L_c + L_t)C_{ot}C_t w^2 - C_{eq}]} \quad (3.6)$$

where $C_{eq} = C_{ot} + C_t$. Consequently, the natural frequency of the system is given by the pole of equation 3.6,

$$\omega_o = \left\{ \frac{C_{eq}}{(L_c + L_t)C_{ot}C_t} \right\}^{\frac{1}{2}} \quad (3.7)$$

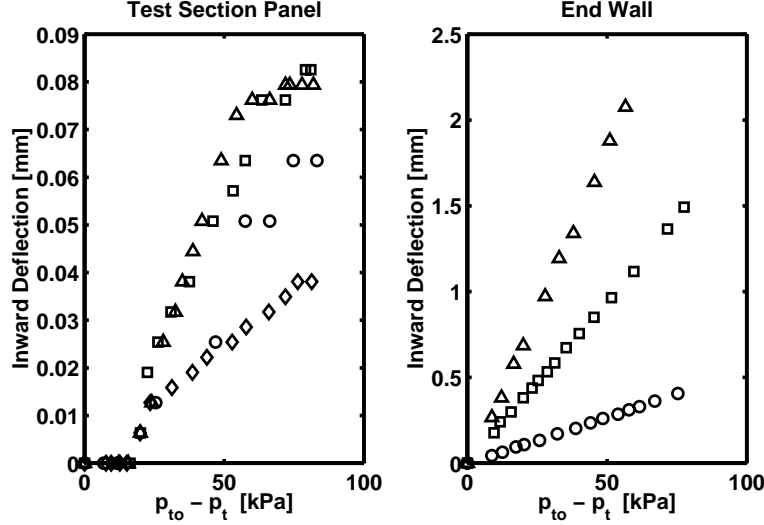


FIGURE 7. Deflection of tunnel walls in response to static changes in the tunnel pressure, p_t , relative to an initial tunnel pressure, p_{to} . The left graph shows the deflection of a front test section panel: at the panel center (\triangle), the panel long edge midpoint (\square), the panel short edge midpoint (\circ), and the panel corner (\star). The right graph shows the deflection of the tunnel end wall near the downstream turning vanes: close to a supporting flange (\triangle) and at two more distant points (\square, \circ).

The estimated values of the lumped parameters indicate that $L_c \gg L_t$, and thus this natural frequency is very nearly

$$\omega_o \approx \left\{ \frac{1}{L_c} \left(\frac{1}{C_{ot}} + \frac{1}{C_t} \right) \right\}^{\frac{1}{2}} = \left\{ \frac{1}{L_c} \left(\frac{g}{\bar{A}_{ot}} + \frac{\bar{p}_{ot} k}{\rho \bar{V}_{ot}} + \frac{1}{C_t} \right) \right\}^{\frac{1}{2}} \quad (3.8)$$

Inspection of this equation (Duttweiler 2001) revealed that the natural frequency is dominated by the tunnel compliance. This is confirmed in figure 8, which shows the natural frequency predicted by equation 3.8 as a function of overflow tank pressure. Also shown in figure 8 are experimentally determined natural frequencies, found by perturbing the system pressure with a rapid valve closure and then monitoring the resulting pressure fluctuations.

The curve corresponding to the tunnel compliance value of $C_t = 2.9 \times 10^{-4} \text{ m}^2$ is in good agreement with the experimentally determined natural frequency at higher overflow tank pressures. However, the calculated natural frequencies do not show the same degree of variation with overflow tank pressure as exhibited by the experimental data. This suggests that the tunnel compliance may not be constant as the pressure is varied.

3.3. Forced Response Experiments

The proposed model for the system impedance can be further assessed by experimentally measuring the response of the facility to a volumetric excitation. This was achieved using an oscillating piston setup (see Duttweiler 2001), where the output from the piston (bore diameter 38 mm) was directed through an essentially rigid pipe into the test section. The resulting pressure fluctuations were measured using a transducer mounted in the ceiling of the test section approximately 0.51 m upstream. Figure 9 shows the system impedance determined from these pressure measurements, at various excitation frequencies and piston strokelengths, $|\tilde{x}_p|$. Figure 10 presents the data at higher frequencies.

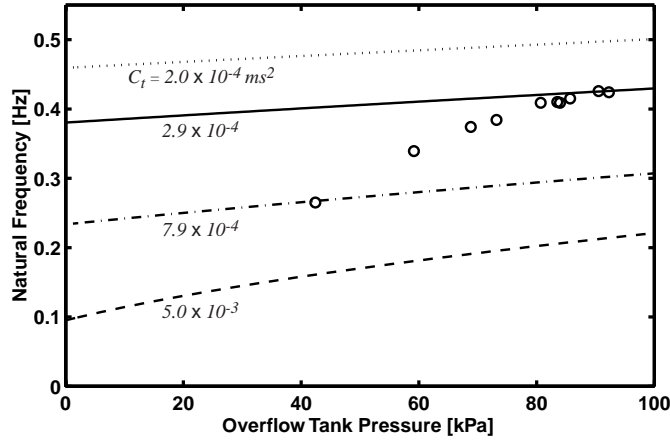


FIGURE 8. The variation of the natural frequency with overflow tank pressure (O) and the predictions of equation 3.8 for several values of the tunnel compliance, C_t .

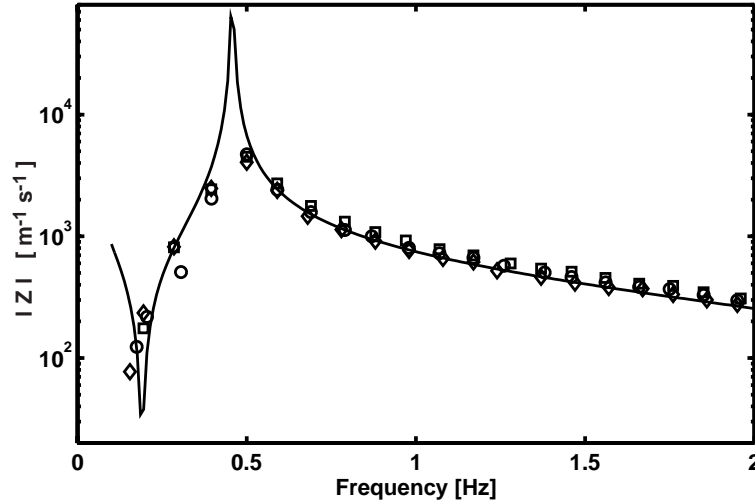


FIGURE 9. Magnitude of system impedance at low frequencies for $|\hat{x}_p| = 6.5$ (O), 12.4 (Δ), and 15.7 mm (\square). Also, equation 3.6 (—) is plotted for a value of $L_t = 6.75$ m^{-1} .

Also shown in figure 9 is the prediction of the model, which accurately captures the minimum in the experimental response at approximately $f = 0.2$ Hz, corresponding to the zero of equation 3.6 at

$$\omega_z = \left\{ \frac{1}{L_c C_{ot}} \right\}^{\frac{1}{2}} \quad (3.9)$$

Since this line in figure 9 is generated using the value of the tunnel compliance determined from the natural frequency experiments, it is not surprising the the model also accurately captures the resonant behavior at approximately 0.5 Hz. Finally, the model also captures the minimum at higher frequencies, shown in figure 10, corresponding to the second zero

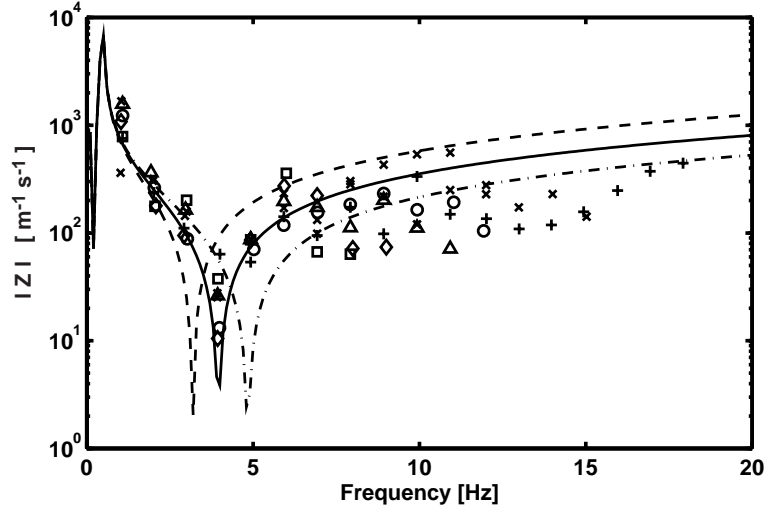


FIGURE 10. Magnitude of system impedance at high frequencies for various piston amplitudes, $|\hat{x}_p| = 1.6$ (+), 2.9 (x), 6.5 (O), 9.0 (Δ), 12.4 (\triangle), and 15.7 mm (\square). Also, equation 3.6 is plotted for values of $L_t = 4.50$ ($\cdot - \cdot$), 6.75 ($-$), and 10.4 m^{-1} ($- -$).

at

$$\omega_z = \left\{ \frac{1}{L_t C_t} \right\}^{\frac{1}{2}} \quad (3.10)$$

Note that since C_t has already been determined from the natural frequency experiments, this relation only contains one unconfirmed quantity, namely the tunnel inertance, L_t . The figure includes model results for several different values of L_t all of which are in a range consistent with the water tunnel geometry.

Experiments were also conducted to measure the phase of the pressure fluctuations induced by the oscillating piston (see Duttweiler 2001). As would be expected, both the experimentally determined phase and the predictions of equation 3.6 exhibit phase transitions at the low frequency zero and again at resonance.

4. Cavitation Dynamics

The preceding experiments demonstrate that the test section flow conditions will respond to the volumetric excitations imposed by a fluctuating cavity volume in the tunnel test section. Yet, the cavity volume itself responds to changes in the test section flow conditions. Clearly then, the cavitation dynamics and facility dynamics must be considered as part of a coupled system.

Essential to understanding these coupled dynamics is determining how the cavity volume responds to changing inlet conditions. As described earlier, analytical studies of two-dimensional hydrofoils show that the non-dimensional cavity length, l/c , is approximately a function of the ratio of the effective angle of attack to the cavitation number, α/σ . Furthermore, since as proposed by Blake (1986) the cavity volume is proportional to the propeller radius and the square of the cavity length, the total cavity volume is also essentially a function of the ratio α/σ .

At a given propeller speed, the effective angle of attack α is determined entirely by the mass flow rate approaching the propeller, m_t , while the cavitation number is determined entirely by the test section pressure, p_t . It is therefore appropriate to express the variation

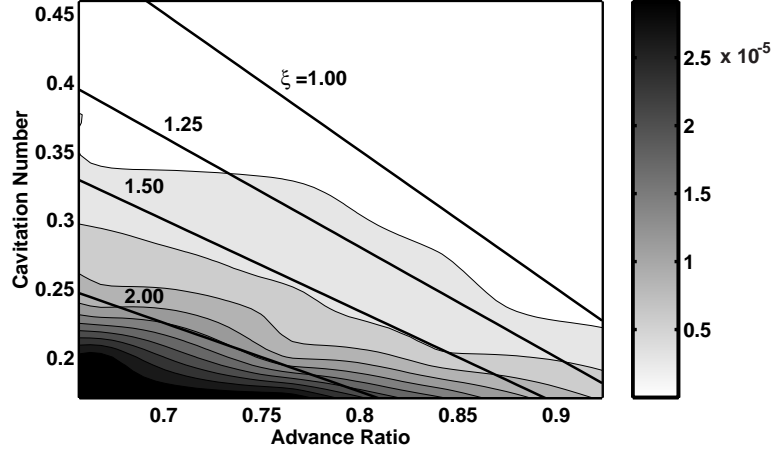


FIGURE 11. Cavity volume on propeller blades at intermediate rotation speed ($n = 28.3 \text{ Hz}$). The gray scale on the right indicates the cavitation volume in m^3 . The lines in the map are lines of constant ξ as indicated.

in cavity volume with α and σ in terms of a cavitation compliance $K = -\rho(dV_{cav}/dp_t)_{m_t}$ and a mass flow gain factor $M = -\rho(dV_{cav}/dm_t)_{p_t}$ (Brennen 1994). To effect this, it is convenient to recast these dynamic characteristics in terms of the parameters more frequently used in cavitating propeller experiments, namely the advance ratio, J , and the cavitation number, σ :

$$K \doteq -\rho \left(\frac{dV_{cav}}{dp_t} \right)_{m_t} = -\frac{2}{\Omega^2 R^2} \left(\frac{dV_{cav}}{d\sigma} \right)_J \quad (4.1)$$

$$M \doteq -\rho \left(\frac{dV_{cav}}{dm_t} \right)_{p_t} = -\frac{\pi}{A_t \Omega R} \left(\frac{dV_{cav}}{dJ} \right)_\sigma \quad (4.2)$$

where $\Omega = 2\pi n$ is the radian frequency of the propeller rotation, R is the radius of the propeller, and A_t is the test section cross-sectional area.

It is valuable to determine quasi-static values for K and M using the experimental data for the cavity volume as a function of J and σ . Figure 11 shows the results from such a set of experiments. Since the cavity length is essentially a function of the parameter $\xi = (J_o - J)/\sigma$, it follows that the cavity volume will also be a function of this single parameter. Accordingly, several lines of constant ξ are plotted in figure 11. Then, given the good correspondence between lines of constant ξ and the experimentally determined contours of constant volume, it is convenient to fit the cavity volume to a function of the form $V_{cav} = h(\xi)$. Choosing a second order polynomial $h(\xi) = a\xi^2 + b\xi + c$, equations 4.1 and 4.2 yield

$$K = \frac{2}{\Omega^2 R^2 \sigma} (2a\xi^2 + b\xi) \quad ; \quad M = \frac{\pi}{A_t \Omega R \sigma} (2a\xi + b) \quad (4.3)$$

where $a = 0.86 \times 10^{-5} \text{ m}^3$ and $b = -1.2 \times 10^{-5} \text{ m}^3$.

To facilitate comparison with results obtained by previous investigators exploring the unstable behavior of cavitating pumps, the dynamic cavitation parameters are non-dimensionalized by

$$K^* = \frac{\Omega^2 K}{R} \quad ; \quad M^* = \Omega M \quad (4.4)$$

It is also necessary to account for the fact that, in the case of a cavitating pump, the mass flow gain factor is based on the mass flow rate entering the cross-sectional area of the pump. In contrast, the definition of equation 4.4 is based on the mass flowing through the cross-sectional area of the entire test section. For appropriate comparison, an adjustment is necessary, increasing the mass flow gain factor computed for the propeller by a factor of $\eta = A_t/A_x$, the ratio of the test section area to the area of the propeller disc.

After this adjustment, the ranges of the dimensionless cavitation compliance and dimensionless mass flow gain factor are determined to be $K^* = 0.0 - 1.4$ and $M^* = 0.05 - 0.20$ for the advance ratios and cavitation numbers investigated at $n = 28.3 \text{ Hz}$. At $n = 31.7 \text{ Hz}$, these ranges increase slightly to $K^* = 0.0 - 1.6$ and $M^* = 0.0 - 0.4$. For comparison, in the first estimate of these dynamic parameters for a cavitating inducer, Brennen (1976) obtained values in the ranges of $K^* = 0.05 - 0.2$ and $M^* = 0.6 - 0.8$ for cavitation numbers above $\sigma = 0.02$. Experimental measurements by Brennen *et al.* (1982) for cavitating inducers at $\sigma = 0.2$ yielded a larger typical value of $K^* = 0.25$, but similar values of $M^* = 0.6$. More recently, theoretical studies by Otsuka *et al.* (1996) examined the potential frequency dependence of K^* and M^* . At low frequencies and $\sigma = 0.17$, they obtained values of the order of $K^* = 0.06$ and $M^* = 0.6$. All of these values are in reasonable agreement with the current work, since differences would be expected given the geometrical differences between propellers and pumps.

5. Facility and Cavitation Dynamics

The inclusion of the cavitation dynamics significantly alters the character of the overall system dynamics. The nature of this change is most clearly illustrated by considering a simplified system consisting only of a source of fluctuating mass flow rate and the cavitation dynamics discussed in section 4. If the outlet of the propeller is assumed closed to fluctuations in mass flow rate, then the impedance of this system is given by

$$Z = \frac{1 - j\omega M}{j\omega K} \quad \text{and} \quad \text{Re}[Z] = -\frac{M}{K} \quad (5.1)$$

Equations 4.3 and figure 11 indicate that the cavitation compliance and mass flow gain factor are both positive. Therefore, this simplified system is characterized by a negative value of the real part of the system impedance, $\text{Re}[Z]$. Accordingly the system is an active one in that it is capable of sustaining fluctuations without an external input of fluctuation energy, instead extracting the fluctuation energy from the steady flow. This is in accord with the view of other investigators such as Brennen (1978) and Tsujimoto *et al.* (1993) who characterize cavitating pump instabilities as essentially arising from a positive mass flow gain factor.

The effects of this behavior on a more complete model incorporating both the facility and cavitation dynamics can be seen by considering the model presented earlier in figure 6. The system impedance for the location e is:

$$Z = \frac{(L_t C_t \omega^2 - 1) Z_c}{j L_t C_t \{Z_c K - M\} \omega^3 - L_t C_t \left\{ \frac{Z_c M}{L_{tu}} - 1 \right\} \omega^2 + j \{M - Z_c (C_t + K)\} \omega - 1} \quad (5.2)$$

where $L_t^{-1} = L_{tu}^{-1} + L_{td}^{-1}$, and Z_c is the impedance of the connecting pipe and overflow tank,

$$Z_c = j\omega L_c + R_c + \frac{1}{j\omega C_{ot}} \quad (5.3)$$

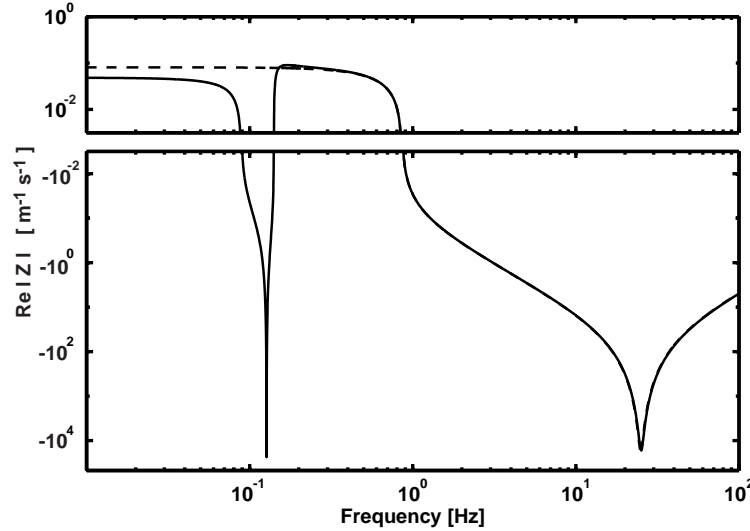


FIGURE 12. Real part of system impedance, Z , for the combined facility and cavitation dynamics model. Shown are the results of the full model of figure 6 (—) and a simplified model neglecting the overflow tank and connecting pipe dynamics (---).

Figure 12 plots the real part of this system impedance as a function of frequency. In generating this plot, values of $K = 5.9 \times 10^{-6} \text{ ms}^2$ and $M = 5.9 \times 10^{-4} \text{ s}$ were obtained from equations 4.3. The value for the tunnel compliance, $C_t = 5 \times 10^{-3} \text{ ms}^2$, was chosen based on figure 8 and the reduced overflow tank pressure, $p_{ot} = 18 \text{ kPa}$, required to obtain cavitating conditions. The estimates of section 3.1 were used to evaluate the remaining parameters, though the resistive effects have initially been omitted from the calculation. Curves are generated for the system of figure 6 as well as for a simplified system without the connecting pipe and overflow tank dynamics.

Immediately apparent from figure 12 is that the real part of the system impedance is negative over two frequency ranges centered at approximately $f = 0.12 \text{ Hz}$ and $f = 25 \text{ Hz}$. The active nature of the cavitation dynamics exemplified by Equation 5.1 is still evident, but with the addition of the facility dynamics the positive activity has been limited to these two frequency ranges. The unstable region around 0.12 Hz corresponds to the natural frequency discussed in section 3.2, the low value of 0.12 Hz resulting from the increased value of the tunnel compliance. As would be expected, the curve generated for the simplified system does not exhibit this trough.

The trough at $f = 25 \text{ Hz}$ therefore seems a probable explanation for the propeller instability. At this frequency, the combination of facility and cavitation dynamics results in the creation of fluctuation energy and therefore potentially unstable behavior of the cavitation on the propeller. However, there is a large discrepancy between the frequency of this trough and the typical experimentally observed instability frequency of $f = 10 \text{ Hz}$.

Since both the full and simplified models exhibit similar behavior through this second trough, it is appropriate to further analyze this behavior by considering only the simplified system. The impedance of the simplified system is given by

$$Z = \frac{L_t C_t \omega^2 - 1}{j\omega \left\{ L_t C_t K^* \omega^2 + j \left\{ \frac{L_t}{L_{tu}} \right\} C_t M^* \omega - (C_t + K^*) \right\}} \quad (5.4)$$

A reasonable approximation of the pole location of this impedance is

$$\omega_o = \left\{ \frac{C_t + K^*}{L_t C_t K^*} \right\}^{\frac{1}{2}} \quad (5.5)$$

and, since $C_t \gg K^*$, the pole is essentially determined by

$$\omega_o = \left\{ \frac{1}{L_t K^*} \right\}^{\frac{1}{2}} \quad (5.6)$$

The location of the pole given by this expression is very nearly the location of the trough in the real part of the system impedance shown in figure 12.

As an aside, equation 5.6 can also be applied to cavitating pumps and helps explain the experimental observations of Brennen (1994) that the auto-oscillation frequency for many different impellers is roughly proportional to $\sigma^{\frac{1}{2}}$. Since K^* is roughly inversely proportional to σ (Brennen *et al.* 1982), the predicted auto-oscillation frequency will be proportional to $\sigma^{\frac{1}{2}}$.

Now consider further the discrepancy between the instability frequency and the trough frequency obtained using the current estimate of the cavitation compliance. That value was based only on the variations in cavity volume observed on the propeller blades. However, as noted in the initial observations of the instability, there is also substantial variation in the cavity volume within the tip vortices. If an estimate is made of the tip vortex volume (Duttweiler 2001), it transpires that the cavitation compliance could be increased by as much as a factor of six. Such an increase results in a trough at a frequency of $f = 10.4 \text{ Hz}$. This provides one possible explanation for the discrepancy. Another possibility is that non-linear effects produce a limit cycle frequency which is significantly smaller than the prediction of the linear instability analysis.

The preceding analysis did not include any system resistances. Figure 13 shows the effects on the simplified system of including tunnel resistances. The cavitation compliance is evaluated including the component contributed by the tip vortex cavitation. Three lines are drawn for cases in which the upstream and downstream resistances, R_{tu} and R_{td} , are assumed to be equal. The chosen values for the resistances are characterized by a non-dimensional damping parameter,

$$\zeta = \frac{5R_t K^*}{3M^*} \quad (5.7)$$

where $R_t^{-1} = R_{tu}^{-1} + R_{td}^{-1}$ is an effective resistance based on the parallel combination of the upstream and downstream resistances. This parameter represents a ratio of the resistive effects opposing unstable behavior to the dynamic characteristic driving the instability, namely the quantity M^*/K^* .

It is apparent from figure 13 that the system impedance undergoes a dramatic transition at $\zeta = 1$. The well defined trough transforms into a dramatic positive peak in the real part of the system impedance. For $\zeta > 0$ (for example, $\zeta = 1.25$) the real part of the system impedance becomes negative at higher frequencies, but the amplitude of those negative values is several orders of magnitude lower than that of the trough present when $\zeta < 1$. For sufficiently high values of ζ , the real part of the system impedance remains positive across all frequencies.

If the upstream and downstream resistances are not assumed equal, the behavior of the system impedance becomes significantly more complicated. Figure 13 also shows the real part of the system impedance at various ratios of upstream to downstream tunnel resistance. Despite the fact that all three curves are generated for a damping value of

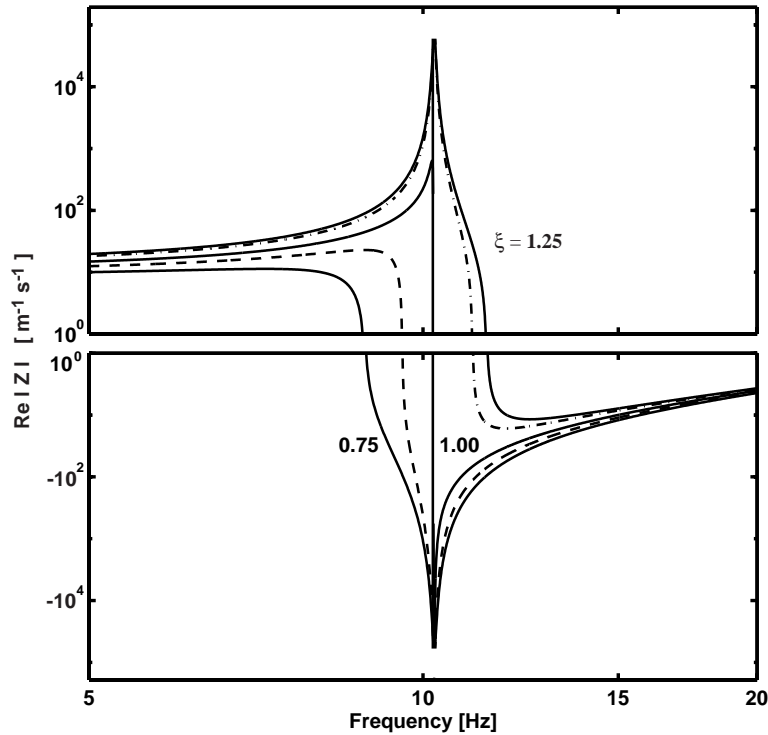


FIGURE 13. Effect of resistance on real part of system impedance, Z , for several values of the parameter ζ (—), including the critical value of $\zeta = 1$ (using $R_{tu} = R_{td}$). Also shown is the effect of unbalanced upstream and downstream resistances, namely $R_{tu}/R_{td} = 0.75$ (—) and 0.75 ($\cdot - \cdot$) (for $\zeta = 1.0$).

$\zeta = 1.0$, the case of a lesser upstream resistance results in unstable behavior. In contrast, a greater upstream resistance results in stable behavior. Thus, the model predicts that unstable behavior is favored by a relatively smaller upstream resistance.

It was pointed out in the introduction that the instability occurred most prevalently when the propeller was mounted downstream of the supporting strut. One speculation was that the strut introduced an asymmetric resistance which promoted the instability but this is clearly not substantiated by the preceding analysis of the effect of unequal resistances. Thus the effect of the supporting strut is, as yet, unexplained. It could simply be that it introduces random perturbations to the flow through the propeller which are amplified through the instability mechanism.

6. Conclusions

This paper has described an investigation of a previously unreported surge instability on a cavitating propeller mounted in a water tunnel. The cyclic behavior of the attached blade cavities has strong similarities to that of partial cavity oscillation on single hydrofoils in that the cavity length oscillates between a configuration in which the length is substantially less than the chord over almost all of the span and one in which a significant fraction of the cavity near the tip is longer than the chord. The reduced frequency of the instability is consistent with the partial cavity instability on single foils. The ampli-

tudes of the pressures generated are large and potentially damaging to the surrounding structure.

To understand the nature of this instability and its source, separate investigations of the cavitation dynamics and of the response of the water tunnel were undertaken. It is demonstrated that the cavitation dynamics may be characterized by an approach previously deployed during identification of the dynamics of cavitating pumps; quasi-static observations of the parametric variations in the cavity volume are then used to quantify the quantities known as the cavitation compliance and the mass flow gain factor. The dynamic response of the tunnel is investigated by inserting known volume oscillations by means of a piston device and a complete model of the linear cavitation dynamics and the tunnel response is then constructed. This model demonstrates that the instability is essentially driven by a positive mass flow gain factor. It predicts instability characteristics (frequencies, etc.) which are mostly in accord with the observations. However, some features of the instability remain unexplained, such as the role of the supporting strut asymmetry; these may be a consequence of unidentified dynamic features of the water tunnel.

Whether or not the instability could occur in the environment downstream of a ship hull would require the construction and analysis of a dynamic model which included both the cavitation characteristics utilized herein as well as a model for the response of the surroundings to the volume oscillations. While the literature contains a number of attempts to model the surroundings (see, for example, Huse 1972, Weitendorf 1989) the authors do not know of any complete model of the type suggested here.

This research program was partly supported by the Office of Naval Research under grant number N00014-91-J-1295. The authors are grateful for the propellers provided by Dr. Stuart Jessup and the David Taylor Model Basin. We also greatly appreciate the advice and encouragement of Professors Allan Acosta and Tim Colonius and the help of Teichi Tanaka, Philip Rodriguez, Dale Parkes and Steve Schell.

REFERENCES

- BARK, G. 1986 Development of violent collapses in propeller cavitation. *ASME Cavitation and Multiphase Flow Forum*, 65-76.
- BLAKE, W. K. 1986 Propeller cavitation noise: the problems of scaling and prediction. *Proc. ASME Int. Symp. on Cavitation and Multiphase Flow Noise*, **FED-45**, 89-100.
- BRAISTED, D.M. & BRENNEN, C.E. 1978 Observations on instabilities of cavitating inducers. *ASME Cavitation and Polyphase Flow Forum*, 19-22.
- BRAISTED, D.M. & BRENNEN, C.E. 1980 Auto-oscillation of cavitating inducers. *Proc. ASME Symp. on Polyphase Flow and Transport Tech.*, 157-166.
- BRENNEN, C.E. 1978 Bubbly flow model for the dynamic characteristics of cavitating pumps. *J. Fluid Mech.*, **89**, 223-240.
- BRENNEN, C. E. 1994 *Hydrodynamics of Pumps*. Oxford University Press and Concepts ETI.
- BRENNEN, C. E. 1995 *Cavitation and bubble dynamics*. Oxford University Press.
- BRENNEN, C.E. & ACOSTA, A.J. 1973 Theoretical, quasistatic analyses of cavitation compliance in turbopumps. *J. Spacecraft and Rockets*, **10** (3), 175-180.
- BRENNEN, C.E. & ACOSTA, A.J. 1976 The dynamic transfer function for a cavitating inducer. *ASME J. Fluids Eng.*, **98**, 182-191.
- BRENNEN, C.E., MEISSNER, C., LO, E.Y. AND HOFFMAN, G.S. 1982 Scale effects in the dynamic transfer functions for cavitating inducers. *ASME J. Fluids Eng.*, **104**, 428-433.
- DUTTWEILER, M.E. 2001 Surge instability on a cavitating propeller. Ph.D. thesis, California Institute of Technology.
- DE LANGE, D.F., DE BRUIN, G.J. & VAN WIJNGAARDEN, L. 1994 On the mechanism of cloud cavitation - experiment and modeling. In *Proc. 2nd Int. Symp. on Cavitation, Tokyo*, 45-50.

- FRANC, J. P. & MICHEL, J. M. 1988 Unsteady attached cavitation on an oscillating hydrofoil. *J. Fluid Mech.* **193**, 171–189.
- GATES, E.M. 1977 The influence of free stream turbulence, free stream nuclei populations, and a drag-reducing polymer on cavitation inception on two axisymmetric bodies. Ph.D. thesis, Cal. Inst. of Tech.
- HART, D.P., BRENNEN, C.E. & ACOSTA, A.J. 1990 Observations of cavitation on a three dimensional oscillating hydrofoil. *ASME Cavitation and Multiphase Flow Forum*, **FED-98**, 49–52.
- HUSE, E. 1972 Pressure fluctuations on the hull induced by a cavitating propeller. *Tech. Rep.*, 111, Norwegian Ship Model Experiments Tank.
- JESSUP, S. 1997 Cavitation on the 4990 hydrofoil. Private communication.
- KJELDSSEN, M., VENNATRO, R., ARNDT, R. AND KELLER, A. 1999 Discussion on cyclic cavitation in closed water tunnels and the influence from the dynamic response of the tunnel. *Proc. IAHR Working Group on Behavior of Hyd. Machinery under Steady Oscillating Conditions*.
- LABERTEAUX, K. & CECCIO, S.L. 1998 Partial attached cavitation on two- and three-dimensional hydrofoils. *Proc. 22nd ONR Symp. on Naval Hydrodynamics*, 239–254.
- LE, Q., FRANC, J. M. & AND MICHEL, J. M. 1993 Partial cavities: global behaviour and mean pressure distribution. *ASME J. Fluids Eng.* **115**, 243–248.
- McKENNEY, E.A. 1995 A study of tip vortices and cavitation on a propeller in a non-uniform flow field. Ph.D. thesis, California Institute of Technology.
- McKENNEY, E.A. AND BRENNEN, C.E. 1994 On the dynamics and acoustics of cloud cavitation on an oscillating hydrofoil. In *Proc. ASME Symp. on Cavitation and Gas-Liquid Flows in Fluid Machinery and Devices*, **FED-190**, 195–202.
- NG, S.L. & BRENNEN, C.E. 1978 Experiments on the dynamic behavior of cavitating pumps. *ASME J. Fluids Eng.*, **100**, 166–176.
- OTSUKA, S., TSUJIMOTO, Y., KAMIJO, K. AND FURUYA, O. 1996 Frequency dependence of mass flow gain factor and cavitation compliance of cavitating inducers. *ASME J. Fluids Eng.*, **118**, 400–408.
- REISMAN, G.E., WANG, Y.-C. & BRENNEN, C.E. 1998 Observations of shock waves in cloud cavitation. *J. Fluid Mech.* **355**, 255–283.
- SHEN, Y. & PETERSON, F. B. 1978 Unsteady cavitation on an oscillating hydrofoil. *Proc. 12th ONR Symp. on Naval Hydrodynamics*, 362–384.
- SOYAMA, H., KATO, H. & OBA, R. 1992 Cavitation observations of severely erosive vortex cavitation arising in a centrifugal pump. *Proc. Third IMechE Int. Conf. on Cavitation*, 103–110.
- TSUJIMOTO, Y., KAMIJO, K. AND YOSHIDA, Y. 1993 A theoretical analysis of rotating cavitation in inducers. *ASME J. Fluids Eng.*, **115**, 135–141.
- TULIN, M.P. 1953 Steady, two-dimensional cavity flows about slender bodies. *Tech. Rep.* 834, David Taylor Model Basin.
- WADE, R. B. & ACOSTA, A. J. 1966 Experimental observations on the flow past a plano-convex hydrofoil. *ASME J. Basic Eng.* **88**, 273–283.
- WEITENDORF, E.A. 1989 25 years research on propeller excited pressure fluctuations and cavitation. *Proc. ASME Int. Symp. on Cavitation Noise and Erosion in Fluid Systems*, **FED-18**, 1–10.